Assessing the Role of Inter-Molecular Interactions in a Perylene-Based Nanowire Using First-Principles Many-Body Perturbation Theory

Tianlun Huang,[1] *D. Kirk Lewis,*[2] *Sahar Sharifzadeh**[1,2,3]

1. Division of Materials and Engineering, Boston University, Boston, Massachusetts 02215, United States

2. Department of Electrical and Computer Engineering, Boston University, Boston, Massachusetts 02215, United States

3. Department of Physics, Boston University, Boston, Massachusetts 02215, United States

*Corresponding Author Email: ssharifz@bu.edu

Abstract

We present a first-principles many-body perturbation theory study of the role of inter-molecular coupling on the optoelectronic properties of a one-dimensional π-stacked nanowire composed of perylene-3,4,9,10-tetracarboxylic diimide (PTCDI) molecules on a DNA-like backbone. We determine that strong inter-molecular electronic coupling results in large bandwidths and low carrier effective masses, suggesting a high electron mobility material. Additionally, by including the role of finite temperature phonons on optical absorption via a newly presented approach, we predict that the optical absorption spectrum at room temperature is significantly altered from room temperature due to allowed indirect transitions, while the exciton delocalization and binding energy, a measure of inter-molecular electronic interactions, remains constant. Overall, our studies indicate that strong inter-molecular coupling can dominate the optoelectronic properties of π-conjugated 1D systems even at room temperature.

TOC Graphic

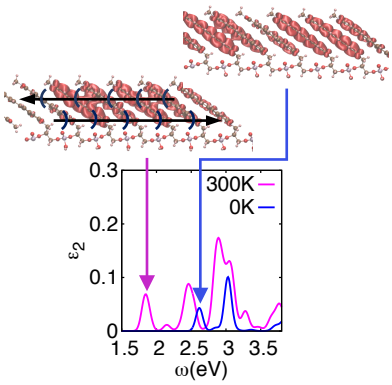

Keywords: GW/BSE; density functional theory; density functional perturbation theory; organic nanowire; electron-phonon interactions; excitons

Organic semiconductors are promising next-generation optoelectronic materials due to their strong light absorption, abundance, flexibility, cheap processing, and chemical tunability.[1–8] In particular, one-dimensional (1D) organic nanowires, consisting of stacked molecular building blocks, have been incorporated as components in field-effect transistors,[9–11] chemical sensors,[12,13] optical waveguides,[14,15] lasers,[16] light emitting diodes,[17] and excitonic circuits.[18,19] These 1D nanowires can be grown via molecular self-assembly with significant control over their inter-molecular structure. This in turn has allowed the design of these materials for high carrier mobility, and efficient light absorption and emission at controllable wavelengths.[20–26]

π-stacked 1D assemblies, in particular, display higher charge carrier mobility than their thin film counterparts,[27,28] and enhanced exciton diffusion lengths.[23,29,30] Importantly, their one-dimensional nature allows exciton motion to be directed in a particular direction,[29] with long-range energy propagation in the form of exciton-polariton migration.[27] To further improve the functionality of these materials, it is necessary to develop a quantitative understanding of the role of inter-molecular interactions on their optoelectronic properties, which can be achieved via theoretical modeling.

First-principles and semi-empirical simulations of excited-states in 1D π-conjugated molecular stacks have shown that inter-molecular orientation strongly influences electronic coupling, and therefore the optoelectronic properties.[31–36] Additionally, an interplay between Coulomb and charge-transfer-mediated coupling can result in a wide range of photophysical behaviors in dimers,[31,32] and extended polymers.[35,36] Computational studies have also shown that vibrational excitations significantly influence the optoelectronic properties of 1D extended molecular stacks,[37–40] with strongly temperature-dependent charge carrier mobilities[37] and strong vibronic coupling in the absorption spectrum.[38–40] However, a quantitative description of how electronic

interactions in 1D π-conjugated stacks are influenced by finite temperature and long-range inter-molecular phonons, is still lacking.

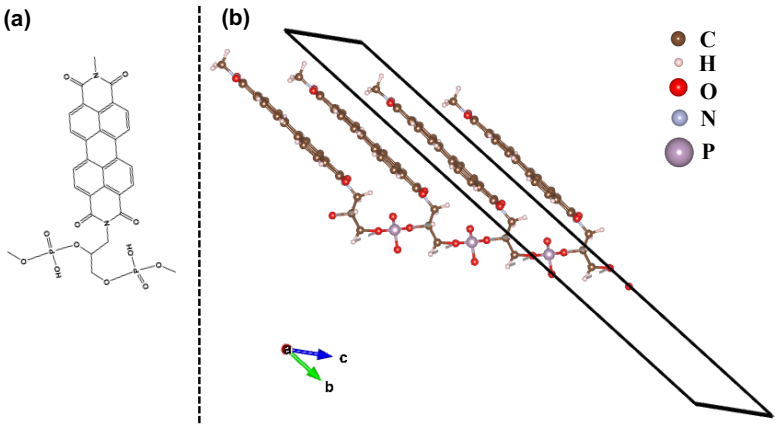

Figure 1. (a) A single Perylene-3,4,9,10 tetracarboxylic diimide (PTCDI) molecule on a phosphoalkane backbone, (b) A nanowire composed of an infinite array of these molecules. The black parallelepiped indicates the unit cell.

In this Letter, we utilize density functional theory (DFT), density functional perturbation theory (DFPT) and many-body perturbation theory (MBPT) to study the optoelectronic properties, including the role of phonons, of a nanowire composed of a biologically inspired perylene-3,4,9,10-tetracarboxylic diimide (PTCDI) derivatives along a DNA-like backbone (Figure 1). PTCDI are a well-studied class of organic materials,[31,41] with a highly tunable inter-molecular spacing and orientation[42] and high electron and exciton mobility.[24] Previous computational and experimental studies of finite stacks of these specific PTCDI derivatives have determined that they possess strong inter-molecular coupling along the π-stack direction with measurements suggesting efficient coherent transport along the stacks.[43,44] In this work, we investigate an extended system (Figure 1b) based on the stacks of Ref.[43] (Figure 1a).

For this artificially constructed but potentially synthesizable nanowire, we determine that there is strong inter-molecular electronic coupling that result in high electron and hole mobility. Additionally, we apply a newly presented approach[45] accounting for the role of finite temperature phonons on the optical properties of materials. Such an approach, to our knowledge, has never been applied to organic systems previously. We determine that at room temperature, long-range inter-molecular phonon-assisted excitations result in a significantly different optical excitation spectrum, with little impact on the nature or binding energy of the exciton. Our study indicates that strong inter-molecular electronic coupling lasts at finite temperature, suggesting that organic nanowires synthesized with significant π-stacking can retain their electronic coherence at finite temperature.

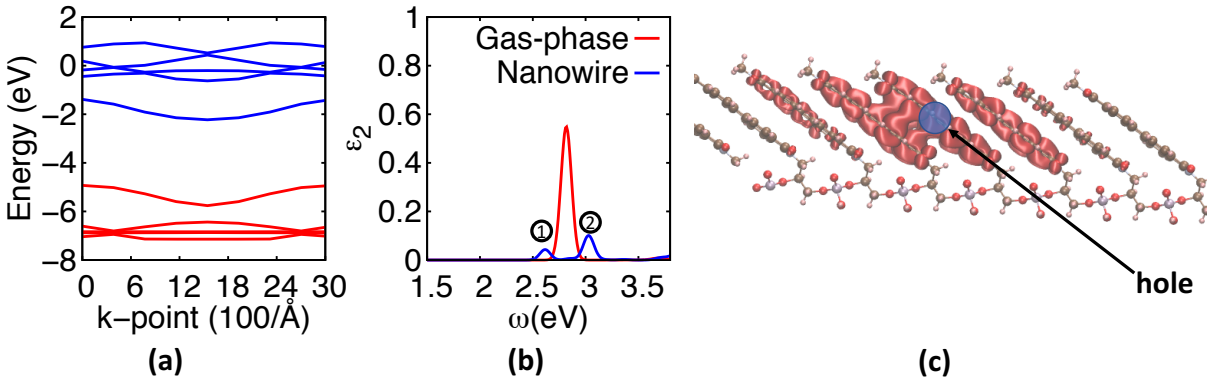

Figure 2. The optical and electronic structure of the nanowire and molecule at T = 0K, excluding zero-point vibrations. (a) Band structure of the nanowire within the GW approximation with valence states in red and conduction states in blue. (b) The optical absorption spectrum of the gas-phase molecule and the nanowire. (c) Exciton distribution for the lowest energy excitation at 2.3 eV with the hole placed slightly above a carbon atom within the PTCDI plane.

First, we examine the electronic and optical properties of the nanowire at zero temperature, with the optical spectrum compared to the gas-phase. The gas-phase molecule is taken from

those previously synthesized (Ref.[43]); while the extended nanowire (Figure 1b) was created such that the inter-molecular spacing and stacking is consistent with the synthesized dimer but that periodic boundary conditions are applied. Due to the presence of the backbone, the spacing between molecules is confined to ~ 3.5 Å, which is quite close for van der Waals-interacting molecules. The strong π-π overlap in this structure results in strong electronic interactions as is evident by the dispersive bandwidths as shown in Figure 2a.

For the nanowire, the fundamental gap, defined as the difference between the electron affinity and ionization potential, is indirect; the computed valence band maximum (VBM) is at the Gamma point while the conduction band minimum (CBM) is at the edge of the first Brillouin zone. The magnitude of the gap is predicted to be 2.7 eV in the nanowire, which is much smaller than that predicted for the gas-phase molecule (4.8 eV). The lowering of the gap in the wire can be partially explained by increased screening in the condensed phase;[46] however, this is a weakly screening 1D system with a calculated average dielectric constant ~ 1.5. The dominant reason for the lower fundamental gap is explained by the formation of dispersive bands; the predicted valence band (VB) and conduction band (CB) bandwidths are both 0.8 eV.

The strong inter-molecular electronic interactions suggest that this material may display high carrier mobility. In order to assess the electron and hole mobilities, we compute the effective mass for electron and hole as $m_{e/h}{}^{*} = \frac{\hbar^2}{\frac{\partial^2 E_{c/v(k)}}{\partial k^2}}$. The carriers are found to be quite light with both approximately 0.08m_e for the hole and electron, where m_e is the free electron mass. Such small effective masses are consistent with previous studies showing high carrier mobility in other π-stacked nanowires.[27,28]

Figure 2b presents the optical absorption spectrum of the nanowire compared with the isolated molecule. For the gas-phase molecule, there is one peak in absorption at 2.8 eV, consisting of

three excited-state transitions. For the nanowire, there are two low-energy peaks at around 2.6 eV and 3 eV, consisting of two states (labeled peak 1) and three states (labeled peak 2). The peaks associated with the nanowire display a reduced intensity compared to the gas-phase, indicating a reduction of overlap between electron and hole in the solid-state. Additionally, the lowering of the onset of absorption from 2.8 eV for the gas-phase to 2.3 eV for the nanowire, can be explained by solid-state screening as well delocalization of the excited-state. The latter is illustrated in Figure 2c, which show the exciton distribution for the lowest energy excited-state within the nanowire, with the hole confined to a high probability location and the electron density plotted. The electron density is delocalized over multiple molecules, as expected for a system with strong π-orbital interactions[47].

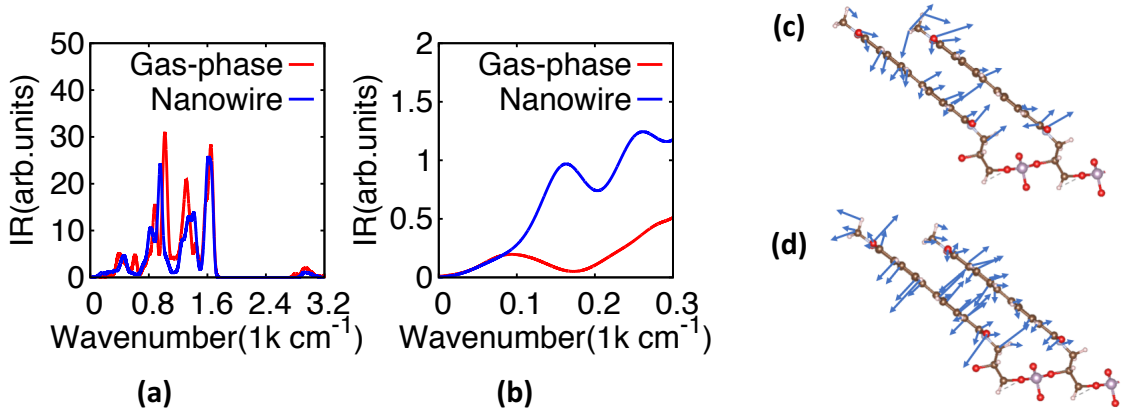

Figure 3. (a) Comparison of the IR spectrum of the gas-phase molecule and nanowire. (b) Zoomed IR spectra from 0 to 300 cm^{-1}. (c-d) Two low energy vibrational modes that dominate the ZG geometry.

In order to understand whether the strong electronic interactions and excited-state delocalization hold at finite temperature, we study the role of room temperature atomic vibrations and long-range phonons on the properties of the nanowire. We first perform a comparison of the phonon normal modes for the extended system and isolated molecule (Figure

3a-b) to understand the changes in vibrational spectra upon formation of the extended system. The IR spectrum for the gas-phase molecule displays peaks characteristic of intra-molecular C=C and C-H stretching modes, as well as C-H rocking, at 850-1050 cm^{-1} and 1400-1600 cm^{-1}, and the characteristic C-H stretch at 3000 cm^{-1}, consistent with other studies of PTCDI derivatives.[48,49] The IR spectrum of the nanowire is similar to that of the isolated molecule for wavenumber greater than 1400 cm^{-1}. Below this frequency, the phonon modes of the nanowire can be decomposed into two regions: intra-molecular vibrations modulated by the backbone (~ 800-1000 cm^{-1}) and inter-molecular vibrations (below 500 cm^{-1}). In the intra-molecular vibration dominant region, the peak shapes for the nanowire are similar to that of the molecule, but the peaks are shifted to lower energies by (~ 60 cm^{-1}). This may be explained by a weakened intra-molecular C=C bond due to the inter-molecular π- interactions; the inter-molecular π-orbital interaction weakens the double bond such that it requires less energy for intra-molecular bond-stretching.[50] In the lower energy region below 300 cm^{-1}, the vibrational modes include out-of-plane motion of the carbon atom, as well as molecular rotation and backbone motion, with many inter-molecular modes in the nanowire that do not exist in the gas-phase, resulting in higher IR intensities in this region for the wire.

We then compute the optoelectronic properties of the nanowire at T = 300K computed via the method introduced by Zacharias and Giustino (ZG).[45] As described in the Computational Details, by this method, phonons are accounted for in the calculated optical spectrum by considering a structural re-organization of the nanowire due to phonons. The optical spectrum associated with the distorted structure approximates the finite temperature optical spectrum. Using this approach, we predict a slight geometry re-organization of the nanowire, with an average displacement of 0.2 Å per atom; this structural reorganization is dominated by low-energy, long-range phonon

modes, indicating that these modes will couple to the excited state. The two modes with the highest contribution are shown in Figure 3c-d. Both modes are low energy inter-molecular modes with energies less than 67 cm^{-1}. The displacement associated with all other phonon modes is smaller than these two by a factor of 1.5 or larger, suggesting that the optically excited-state couples most strongly to these inter-molecular phonons, rather than intra-molecular C=C stretch modes, as would be expected for an isolated molecule.

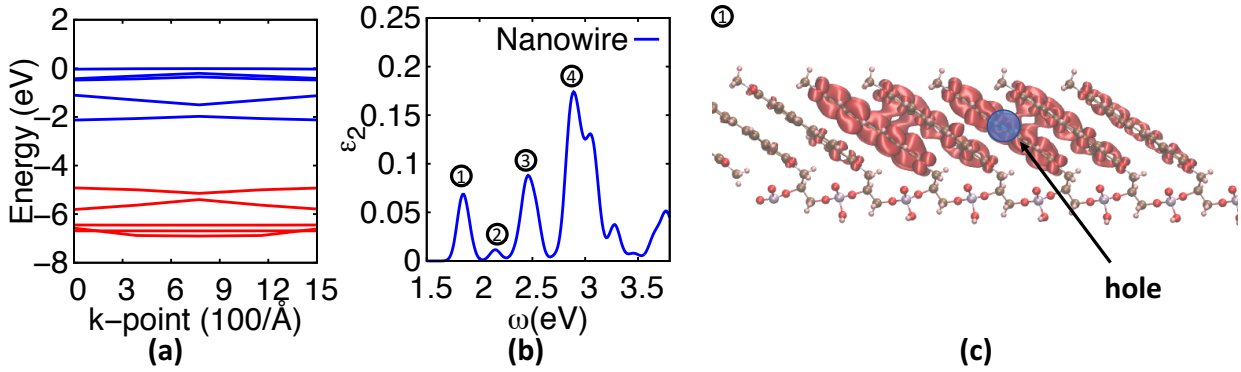

Figure 4. The optical and electronic structure of the nanowire at T = 300K. (a) GW-calculated band structure with valence states in red and conduction states in blue. (b) GW/BSE calculated optical absorption spectrum. (c) Exciton distribution for the lowest energy excited-state at 1.8 eV, with the hole placed slightly above a carbon atom within the distorted PTCDI plane.

The role of room temperature on excitations within the PTCDI nanowire is summarized in Figure 4 and Table 1. The predicted band structure for the ZG structure (Figure 4 a) is direct, with a fundamental gap of 2.8 eV. We note here that the band structure of the nanowire is not direct at finite temperature but the ZG structure accounts for the presence of phonons, which allow the indirect gap to be traversed. Additionally, as shown in Figure 4a, due to the breaking of symmetry between equivalent molecules in the wire, the VB and CB each split into two nearly-degenerate bands. The energy range covered by both bands is 0.9 (1.0) eV for the VB (CB),

consistent with the bandwidths of the 0K structure, suggesting that the strong electronic interactions are preserved.

Figure 4b shows that the optical spectrum of the nanowire at 300K is shifted to lower energies, with multiple peaks within the 0-4 eV energy window. The onset of absorption is at 1.8 eV, 0.5 eV lower than at 0K because the presence of phonons provides the momentum necessary for indirect excitations to occur. Analysis of the exciton wavefunction for the lowest energy state indicates an excitonic state that is delocalized over several molecules, consistent with that of the T = 0K structure. Moreover, the exciton binding energy, calculated as the difference in onset of absorption between the system with electron-hole interactions and one without, is predicted to be 1.2 eV at 0K and 1.0 eV at 300K. The large value of the exciton binding energy is consistent with the weak screening of electron-hole Coulomb interactions within the material. The preservation of the exciton binding energy and exciton extent at finite temperature suggests that the strong inter-molecular electronic interactions are not significantly disrupted at finite temperature.

Table 1. Optical gaps and exciton binding energies* of the nanowire at T = 0K and 300K.

	Optical Gap (eV)	**Exciton Binding Energy (eV)**
T = 0 K	2.3	1.1
T= 300K	1.8	1.0

* The exciton binding is calculated as the energy difference between the onset of absorption with and without electron-hole interactions and is not in reference to the fundamental gap.

In summary, we investigated the optoelectronic properties of a nanowire composed of PTCDI derivatives using density functional theory and many-body perturbation theory, including a novel approach for calculating temperature-dependent optical absorption spectra. At T = 0K, we

predict that strong inter-molecular electronic interactions due to π-orbital stacking lead to high bandwidth and low effective mass, suggesting high conductivity nanowires. Additionally, we examined the change in fundamental and optical gaps upon formation of a one-dimensional condensed phase, and showed that the weak screening of the Coulomb interaction in 1D results in higher exciton binding energies than for typical bulk organic materials. Lastly, we quantitatively determined the change of the nanowire properties under the influence of atomic vibrations and phonons, applying a new approach to electron-phonon interactions that has not been previously applied to organic materials. This analysis revealed that at T = 300 K, the presence of phonons allows indirect transitions to occur, resulting in a lowered optical gap, while the exciton delocalization and binding energy remained constant. Our studies indicate that strong inter-molecular coupling can dominate the optoelectronic properties of organic π-stacked materials even at room temperature.

Computational Details

DFT calculations were performed using the Quantum Espresso package[51] with the Perdew-Burke-Ernzerhof (PBE) approximation to the exchange-correlation.[52] Norm-conserving Troullier-Martins pseudopotentials[53] describe the core and nuclei of atoms with 1, 4, 5, 5, and 6, electrons explicitly considered valence for H, C, N, P, and O, respectively. For the gas-phase molecule (Figure 1 a) the wave function cutoff energy for geometry optimization was 120 Ry, while for subsequent MBPT calculations it was set to 80 Ry, converging the total energy to 2.9 meV/atom and 7 meV/atom, respectively. The isolated molecule was placed in a cubic box with side length of 26.5 Å and the geometry optimized within DFT with a force convergence threshold of 3.4 x 10^{-4} eV/atom. For the nanowire, the Grimme-D2 van der Waals correction[54] was utilized for

geometry optimization, with a force convergence threshold of 5 x 10^{-2} eV/Å. A wave function cutoff energy of 120 Ry and k-point sampling of 1 x 1 x 3 were used, ensuring that the total DFT energy was converged to within 2 meV/atom. The relaxed unit cell size for the nanowire was 6.0 Å x 39.1 Å x 13.9 Å, with the molecular stacks being approximately 3.5 Å apart in a face-to-face orientation.

The vibrational normal modes of both molecule and nanowire were computed using density functional perturbation theory (DFPT)[55] within the Quantum Espresso package, with a q-point grid of 1 x 1 x 2 used for the nanowire.

MBPT calculations within the GW/BSE approximation[56,57] for both isolated molecule and nanowire were performed using the BerkeleyGW[58] package with a PBE starting point. The static dielectric matrix was calculated within the random phase approximation (RPA) and extended to finite frequency with a generalized plasmon pole (GPP) approximation.[59] Due to the imposed periodic boundary conditions, the molecule was placed in a supercell, with lattice vectors along the non-periodic directions that are twice the size necessary to contain 99% of the charge density. In order to minimize the spurious interactions between periodic images, the Coulomb potential was truncated at half of the supercell length. The number of empty states for the molecule and the nanowire in the GW sum was set to 4880 and 4000, respectively, with convergence described in the SI. The neutral excitation energies solved by Bethe-Salpeter equation (BSE) use the Tamm-Dancoff approximation[57] with 24 valence and 24 conduction bands included in the summation for both the molecule and the nanowire. For the nanowire, GW and BSE calculations were performed on a k-point grid of 1x1x8.

To understand the temperature-dependence of optical absorption of the nanowire, we utilized a recently introduced approach by Zacharias and Giustino (ZG),[45] which describes the role of finite

temperature on the dielectric response of materials via an approximation to the Williams[60] and Lax[61] (WL) theory. In short, the imaginary component of the temperature-dependent dielectric function can be approximated as $\epsilon_2(\omega;T) = \prod_\nu \int dx_\nu \frac{\exp(-x_\nu^2/2\sigma_{\nu,T}^2)}{\sqrt{2\pi}\sigma_{\nu,T}} \epsilon_2(\omega;x)$ where x_ν is the normal mode coordinate, $\sigma_{\nu,T}^2$ is a Gaussian broadening, $\frac{\exp(-x_\nu^2/2\sigma_{\nu,T}^2)}{\sqrt{2\pi}\sigma_{\nu,T}}$ is the importance function for Monte Carlo integration, and $\epsilon_2(\omega;x)$ is evaluated at clamped nuclei. In the limit of a large supercell, one single distorted atomic configuration is sufficient to produce the temperature-dependent dielectric function;[45] the atomic displacements for this configuration are determined from normal mode analysis $\Delta\tau_{\kappa\alpha} = (M_P/M_\kappa)^{\frac{1}{2}} \sum_\nu (-1)^{\nu-1} e_{\kappa\alpha,\nu}\sigma_{\nu,T}$ where M_P as the proton mass and M_κ the mass of the κth nucleus.

This analysis is performed within a modified q2r.x subroutine of Quantum Espresso obtained from the authors.[45] For our study, the perturbed average-geometry at room temperature was obtained by skipping the first 22 normal modes in the ZG analysis. Subsequently, the electronic band structure and optical spectrum were obtained by performing GW/BSE calculations and converged with respect to the q-mesh considered. We determined that a 1x1x2 q-mesh is sufficient as shown in the SI.

Acknowledgments

The authors would like to thank Marios Zacharias (Oxford University) and Feliciano Guistino (Oxford University) for access to their software and helpful discussions. This work was supported by the United States National Science Foundation under Award number DMR-161003. Additionally, we acknowledge computational resources from Boston University

Research Computing Services. This work used the Extreme Science and Engineering Discovery Environment (XSEDE) Stampede2 at the service-provider through allocation TG-DMR160012.

Supporting Information

Supporting Information Available: GW convergence plots of the nanowire, the effective mass fit for the hole and electron, and the density of states plots at valence band edge for convergence of the ZG method.

REFERENCES

(1) Cao, W.; Xue, J. Recent Progress in Organic Photovoltaics: Device Architecture and Optical Design. *Energy Environ. Sci.* **2014**, *7* (7), 2123–2144. https://doi.org/10.1039/c4ee00260a.

(2) Scholz, S.; Kondakov, D.; Lüssem, B.; Leo, K. Degradation Mechanisms and Reactions in Organic Light-Emitting Devices. *Chem. Rev.* **2015**, *115* (16), 8449–8503. https://doi.org/10.1021/cr400704v.

(3) Luo, G.; Ren, X.; Zhang, S.; Wu, H.; Choy, W. C. H.; He, Z.; Cao, Y. Recent Advances in Organic Photovoltaics: Device Structure and Optical Engineering Optimization on the Nanoscale. *Small* **2016**, *12* (12), 1547–1571. https://doi.org/10.1002/smll.201502775.

(4) Jou, J.-H.; Kumar, S.; Agrawal, A.; Li, T.-H.; Sahoo, S. Approaches for Fabricating High Efficiency Organic Light Emitting Diodes. *J. Mater. Chem. C* **2015**, *3* (13), 2974–3002. https://doi.org/10.1039/C4TC02495H.

(5) Xu, R.-P.; Li, Y.-Q.; Tang, J.-X. Recent Advances in Flexible Organic Light-Emitting

Diodes. *J. Mater. Chem. C* **2016**, *4* (39), 9116–9142. https://doi.org/10.1039/C6TC03230C.

(6) Zhou, K.; Dong, H.; Zhang, H.; Hu, W. High Performance N-Type and Ambipolar Small Organic Semiconductors for Organic Thin Film Transistors. *Phys. Chem. Chem. Phys.* **2014**, *16* (41), 22448–22457. https://doi.org/10.1039/C4CP01700E.

(7) Sirringhaus, H. 25th Anniversary Article: Organic Field-Effect Transistors: The Path Beyond Amorphous Silicon. *Adv. Mater.* **2014**, *26* (9), 1319–1335. https://doi.org/10.1002/adma.201304346.

(8) Gsänger, M.; Bialas, D.; Huang, L.; Stolte, M.; Würthner, F. Organic Semiconductors Based on Dyes and Color Pigments. *Adv. Mater.* **2016**, *28* (19), 3615–3645. https://doi.org/10.1002/adma.201505440.

(9) Briseno, A. L.; Mannsfeld, S. C. B.; Lu, X.; Xiong, Y.; Jenekhe, S. A.; Bao, Z.; Xia, Y. Fabrication of Field-Effect Transistors from Hexathiapentacene Single-Crystal Nanowires. *Nano Lett.* **2007**, *7* (3), 668–675. https://doi.org/10.1021/nl0627036.

(10) Ghosh, P.; Datta, K.; Mulchandani, A.; Han, S.-H.; Koinkar, P.; Shirsat, M. D. Poly(o -Toluidine) Nanowires Based Organic Field Effect Transistors: A Study on Influence of Anionic Size of Dopants and SWNTs as a Dopant. *J. Phys. Chem. C* **2013**, *117* (29), 15414–15420. https://doi.org/10.1021/jp404674j.

(11) Fleet, L. R.; Stott, J.; Villis, B.; Din, S.; Serri, M.; Aeppli, G.; Heutz, S.; Nathan, A. Self-Assembled Molecular Nanowires for High-Performance Organic Transistors. *ACS Appl. Mater. Interfaces* **2017**, *9* (24), 20686–20695. https://doi.org/10.1021/acsami.7b01449.

(12) Naddo, T.; Che, Y.; Zhang, W.; Balakrishnan, K.; Yang, X.; Yen, M.; Zhao, J.; Moore, J. S.; Zang, L. Detection of Explosives with a Fluorescent Nanofibril Film. *J. Am. Chem. Soc.* **2007**, *129* (22), 6978–6979. https://doi.org/10.1021/ja070747q.

(13) Che, Y.; Yang, X.; Loser, S.; Zang, L. Expedient Vapor Probing of Organic Amines Using Fluorescent Nanofibers Fabricated from an N-Type Organic Semiconductor. *Nano Lett.* **2008**, *8* (8), 2219–2223. https://doi.org/10.1021/nl080761g.

(14) Takazawa, K.; Kitahama, Y.; Kimura, Y.; Kido, G. Optical Waveguide Self-Assembled from Organic Dye Molecules in Solution. *Nano Lett.* **2005**, *5* (7), 1293–1296. https://doi.org/10.1021/nl050469y.

(15) Bao, Q.; Goh, B. M.; Yan, B.; Yu, T.; Shen, Z.; Loh, K. P. Polarized Emission and Optical Waveguide in Crystalline Perylene Diimide Microwires. *Adv. Mater.* **2010**, *22* (33), 3661–3666. https://doi.org/10.1002/adma.201000731.

(16) O'Carroll, D.; Lieberwirth, I.; Redmond, G. Microcavity Effects and Optically Pumped Lasing in Single Conjugated Polymer Nanowires. *Nat. Nanotechnol.* **2007**, *2* (3), 180–184. https://doi.org/10.1038/nnano.2007.35.

(17) Berggren, M.; Inganäs, O.; Gustafsson, G.; Rasmusson, J.; Andersson, M. R.; Hjertberg, T.; Wennerström, O. Light-Emitting Diodes with Variable Colours from Polymer Blends. *Nature* **1994**, *372* (6505), 444–446. https://doi.org/10.1038/372444a0.

(18) High, A. A.; Novitskaya, E. E.; Butov, L. V.; Hanson, M.; Gossard, A. C. Control of Exciton Fluxes in an Excitonic Integrated Circuit. *Science (80-.).* **2008**, *321* (5886), 229–231. https://doi.org/10.1126/science.1157845.

(19) Becker, K.; Lupton, J. M.; Müller, J.; Rogach, A. L.; Talapin, D. V.; Weller, H.; Feldmann, J. Electrical Control of Förster Energy Transfer. *Nat. Mater.* **2006**, *5* (10), 777–781. https://doi.org/10.1038/nmat1738.

(20) Zang, L.; Che, Y.; Moore, J. S. One-Dimensional Self-Assembly of Planar π-Conjugated Molecules: Adaptable Building Blocks for Organic Nanodevices. *Acc. Chem. Res.* **2008**, *41* (12), 1596–1608. https://doi.org/10.1021/ar800030w.

(21) Zhao, Y. S.; Fu, H.; Peng, A.; Ma, Y.; Liao, Q.; Yao, J. Construction and Optoelectronic Properties of Organic One-Dimensional Nanostructures. *Acc. Chem. Res.* **2010**, *43* (3), 409–418. https://doi.org/10.1021/ar900219n.

(22) Chen, S.; Slattum, P.; Wang, C.; Zang, L. Self-Assembly of Perylene Imide Molecules into 1D Nanostructures: Methods, Morphologies, and Applications. *Chem. Rev.* **2015**, *115* (21), 11967–11998. https://doi.org/10.1021/acs.chemrev.5b00312.

(23) Zhang, C.; Yan, Y.; Jing, Y.-Y.; Shi, Q.; Zhao, Y. S.; Yao, J. One-Dimensional Organic Photonic Heterostructures: Rational Construction and Spatial Engineering of Excitonic Emission. *Adv. Mater.* **2012**, *24* (13), 1703–1708. https://doi.org/10.1002/adma.201104326.

(24) Supur, M.; Fukuzumi, S. Energy and Electron Transfer of One-Dimensional Nanomaterials of Perylenediimides. *ECS J. Solid State Sci. Technol.* **2013**, *2* (10), M3051–M3062. https://doi.org/10.1149/2.009310jss.

(25) Cao, X.; Wu, Y.; Fu, H.; Yao, J. Self-Assembly of Perylenediimide Nanobelts and Their Size-Tunable Exciton Dynamic Properties. *J. Phys. Chem. Lett.* **2011**, *2* (17), 2163–2167.

https://doi.org/10.1021/jz2009488.

(26) Kennehan, E. R.; Grieco, C.; Brigeman, A. N.; Doucette, G. S.; Rimshaw, A.; Bisgaier, K.; Giebink, N. C.; Asbury, J. B. Using Molecular Vibrations to Probe Exciton Delocalization in Films of Perylene Diimides with Ultrafast Mid-IR Spectroscopy. *Phys. Chem. Chem. Phys.* **2017**, *19* (36), 24829–24839. https://doi.org/10.1039/C7CP04819J.

(27) Kim, F. S.; Ren, G.; Jenekhe, S. A. One-Dimensional Nanostructures of π-Conjugated Molecular Systems: Assembly, Properties, and Applications from Photovoltaics, Sensors, and Nanophotonics to Nanoelectronics †. *Chem. Mater.* **2011**, *23* (3), 682–732. https://doi.org/10.1021/cm102772x.

(28) Zhou, J.; Zhang, W.; Jiang, X.-F.; Wang, C.; Zhou, X.; Xu, B.; Liu, L.; Xie, Z.; Ma, Y. Magic-Angle Stacking and Strong Intermolecular π–π Interaction in a Perylene Bisimide Crystal: An Approach for Efficient Near-Infrared (NIR) Emission and High Electron Mobility. *J. Phys. Chem. Lett.* **2018**, *9* (3), 596–600. https://doi.org/10.1021/acs.jpclett.7b03251.

(29) Chaudhuri, D.; Li, D.; Che, Y.; Shafran, E.; Gerton, J. M.; Zang, L.; Lupton, J. M. Enhancing Long-Range Exciton Guiding in Molecular Nanowires by H-Aggregation Lifetime Engineering. *Nano Lett.* **2011**, *11* (2), 488–492. https://doi.org/10.1021/nl1033039.

(30) Kaufmann, C.; Bialas, D.; Stolte, M.; Würthner, F. Discrete π-Stacks of Perylene Bisimide Dyes within Folda-Dimers: Insight into Long- and Short-Range Exciton Coupling. *J. Am. Chem. Soc.* **2018**, *140* (31), 9986–9995. https://doi.org/10.1021/jacs.8b05490.

(31) Würthner, F.; Saha-Möller, C. R.; Fimmel, B.; Ogi, S.; Leowanawat, P.; Schmidt, D. Perylene Bisimide Dye Assemblies as Archetype Functional Supramolecular Materials. *Chem. Rev.* **2016**, *116* (3), 962–1052. https://doi.org/10.1021/acs.chemrev.5b00188.

(32) Hestand, N. J.; Spano, F. C. Expanded Theory of H- and J-Molecular Aggregates: The Effects of Vibronic Coupling and Intermolecular Charge Transfer. *Chem. Rev.* **2018**, *118* (15), 7069–7163. https://doi.org/10.1021/acs.chemrev.7b00581.

(33) Vura-Weis, J.; Ratner, M. A.; Wasielewski, M. R. Geometry and Electronic Coupling in Perylenediimide Stacks: Mapping Structure–Charge Transport Relationships. *J. Am. Chem. Soc.* **2010**, *132* (6), 1738–1739. https://doi.org/10.1021/ja907761e.

(34) Zhao, H.-M.; Pfister, J.; Settels, V.; Renz, M.; Kaupp, M.; Dehm, V. C.; Würthner, F.; Fink, R. F.; Engels, B. Understanding Ground- and Excited-State Properties of Perylene Tetracarboxylic Acid Bisimide Crystals by Means of Quantum Chemical Computations. *J. Am. Chem. Soc.* **2009**, *131* (43), 15660–15668. https://doi.org/10.1021/ja902512e.

(35) Kraner, S.; Scholz, R.; Plasser, F.; Koerner, C.; Leo, K. Exciton Size and Binding Energy Limitations in One-Dimensional Organic Materials. *J. Chem. Phys.* **2015**, *143* (24), 244905. https://doi.org/10.1063/1.4938527.

(36) Zhao, H.; Mazumdar, S.; Sheng, C.-X.; Tong, M.; Vardeny, Z. V. Photophysics of Excitons in Quasi-One-Dimensional Organic Semiconductors: Single-Walled Carbon Nanotubes and π -Conjugated Polymers. *Phys. Rev. B* **2006**, *73* (7), 075403. https://doi.org/10.1103/PhysRevB.73.075403.

(37) Idé, J.; Méreau, R.; Ducasse, L.; Castet, F.; Olivier, Y.; Martinelli, N.; Cornil, J.;

Beljonne, D. Supramolecular Organization and Charge Transport Properties of Self-Assembled π-π Stacks of Perylene Diimide Dyes. *J. Phys. Chem. B* **2011**, *115* (18), 5593–5603. https://doi.org/10.1021/jp111422v.

(38) Hestand, N. J.; Kazantsev, R. V.; Weingarten, A. S.; Palmer, L. C.; Stupp, S. I.; Spano, F. C. Extended-Charge-Transfer Excitons in Crystalline Supramolecular Photocatalytic Scaffolds. *J. Am. Chem. Soc.* **2016**, *138* (36), 11762–11774. https://doi.org/10.1021/jacs.6b05673.

(39) Seibt, J.; Winkler, T.; Renziehausen, K.; Dehm, V.; Würthner, F.; Meyer, H.-D.; Engel, V. Vibronic Transitions and Quantum Dynamics in Molecular Oligomers: A Theoretical Analysis with an Application to Aggregates of Perylene Bisimides. *J. Phys. Chem. A* **2009**, *113* (48), 13475–13482. https://doi.org/10.1021/jp904892v.

(40) Hoffmann, M.; Schmidt, K.; Fritz, T.; Hasche, T.; Agranovich, V. M.; Leo, K. The Lowest Energy Frenkel and Charge-Transfer Excitons in Quasi-One-Dimensional Structures: Application to MePTCDI and PTCDA Crystals. *Chem. Phys.* **2000**, *258* (1), 73–96. https://doi.org/10.1016/S0301-0104(00)00157-9.

(41) Huang, C.; Barlow, S.; Marder, S. R. Perylene-3,4,9,10-Tetracarboxylic Acid Diimides: Synthesis, Physical Properties, and Use in Organic Electronics. *J. Org. Chem.* **2011**, *76* (8), 2386–2407. https://doi.org/10.1021/jo2001963.

(42) Balakrishnan, K.; Datar, A.; Oitker, R.; Chen, H.; Zuo, J.; Zang, L. Nanobelt Self-Assembly from an Organic n-Type Semiconductor: Propoxyethyl-PTCDI. *J. Am. Chem. Soc.* **2005**, *127* (30), 10496–10497. https://doi.org/10.1021/ja052940v.

(43) Wardrip, A. G.; Mazaheripour, A.; Hüsken, N.; Jocson, J.-M.; Bartlett, A.; Lopez, R. C.; Frey, N.; Markegard, C. B.; Kladnik, G.; Cossaro, A.; et al. Length-Independent Charge Transport in Chimeric Molecular Wires. *Angew. Chemie Int. Ed.* **2016**, *55* (46), 14267–14271. https://doi.org/10.1002/anie.201605411.

(44) Mazaheripour, A.; Kladnik, G.; Jocson, J.-M.; Wardrip, A. G.; Markegard, C. B.; Frey, N.; Cossaro, A.; Floreano, L.; Verdini, A.; Bartlett, A.; et al. Unexpected Length Dependence of Excited-State Charge Transfer Dynamics for Surface-Confined Perylenediimide Ensembles. *Mater. Horizons* **2017**, *4* (3), 437–441. https://doi.org/10.1039/C6MH00465B.

(45) Zacharias, M.; Giustino, F. One-Shot Calculation of Temperature-Dependent Optical Spectra and Phonon-Induced Band-Gap Renormalization. *Phys. Rev. B* **2016**, *94* (7), 075125. https://doi.org/10.1103/PhysRevB.94.075125.

(46) Sharifzadeh, S.; Biller, A.; Kronik, L.; Neaton, J. B. Quasiparticle and Optical Spectroscopy of the Organic Semiconductors Pentacene and PTCDA from First Principles. *Phys. Rev. B* **2012**, *85* (12), 125307. https://doi.org/10.1103/PhysRevB.85.125307.

(47) Sharifzadeh, S. Many-Body Perturbation Theory for Understanding Optical Excitations in Organic Molecules and Solids. *J. Phys. Condens. Matter* **2018**, *30* (15), 153002. https://doi.org/10.1088/1361-648X/aab0d1.

(48) Kaake, L. G.; Zou, Y.; Panzer, M. J.; Frisbie, C. D.; Zhu, X.-Y. Vibrational Spectroscopy Reveals Electrostatic and Electrochemical Doping in Organic Thin Film Transistors Gated with a Polymer Electrolyte Dielectric. *J. Am. Chem. Soc.* **2007**, *129* (25), 7824–7830. https://doi.org/10.1021/ja070615x.

(49) Kurban, M.; Gündüz, B. Study of Structural, Optical Properties and Electronic Structure of PTCDI-C5 Organic Nanostructure. *Chem. Phys. Lett.* **2018**, *691*, 14–21. https://doi.org/10.1016/j.cplett.2017.10.053.

(50) Reichenbächer, M.; Popp, J. Vibrational Spectroscopy. In *Challenges in Molecular Structure Determination*; Springer Berlin Heidelberg: Berlin, Heidelberg, 2012; pp 63–143. https://doi.org/10.1007/978-3-642-24390-5_2.

(51) Giannozzi, P.; Baroni, S.; Bonini, N.; Calandra, M.; Car, R.; Cavazzoni, C.; Ceresoli, D.; Chiarotti, G. L.; Cococcioni, M.; Dabo, I.; et al. QUANTUM ESPRESSO: A Modular and Open-Source Software Project for Quantum Simulations of Materials. *J. physics. Condens. matter* **2009**, *21* (39), 395502. https://doi.org/10.1088/0953-8984/21/39/395502.

(52) Perdew, J. P.; Burke, K.; Ernzerhof, M. Generalized Gradient Approximation Made Simple. *Phys. Rev. Lett.* **1996**, *77* (18), 3865–3868. https://doi.org/10.1103/PhysRevLett.77.3865.

(53) Troullier, N.; Martins, J. L. Efficient Pseudopotentials for Plane-Wave Calculations. II. Operators for Fast Iterative Diagonalization. *Phys. Rev. B* **1991**, *43* (11), 8861–8869. https://doi.org/10.1103/PhysRevB.43.8861.

(54) Grimme, S. Semiempirical GGA-Type Density Functional Constructed with a Long-Range Dispersion Correction. *J. Comput. Chem.* **2006**, *27* (15), 1787–1799. https://doi.org/10.1002/jcc.20495.

(55) Baroni, S.; de Gironcoli, S.; Dal Corso, A.; Giannozzi, P. Phonons and Related Crystal Properties from Density-Functional Perturbation Theory. *Rev. Mod. Phys.* **2001**, *73* (2),

515–562. https://doi.org/10.1103/RevModPhys.73.515.

(56) Hybertsen, M. S.; Louie, S. G. Electron Correlation in Semiconductors and Insulators: Band Gaps and Quasiparticle Energies. *Phys. Rev. B* **1986**, *34* (8), 5390–5413. https://doi.org/10.1103/PhysRevB.34.5390.

(57) Rohlfing, M.; Louie, S. G. Electron-Hole Excitations and Optical Spectra from First Principles. *Phys. Rev. B* **2000**, *62* (8), 4927–4944. https://doi.org/10.1103/PhysRevB.62.4927.

(58) Deslippe, J.; Samsonidze, G.; Strubbe, D. A.; Jain, M.; Cohen, M. L.; Louie, S. G. BerkeleyGW: A Massively Parallel Computer Package for the Calculation of the Quasiparticle and Optical Properties of Materials and Nanostructures. *Comput. Phys. Commun.* **2012**, *183* (6), 1269–1289. https://doi.org/10.1016/j.cpc.2011.12.006.

(59) Hybertsen, M. S.; Louie, S. G. Ab Initio Static Dielectric Matrices from the Density-Functional Approach. I. Formulation and Application to Semiconductors and Insulators. *Phys. Rev. B* **1987**, *35* (11), 5585–5601. https://doi.org/10.1103/PhysRevB.35.5585.

(60) Williams, F. E. Theoretical Low Temperature Spectra of the Thallium Activated Potassium Chloride Phosphor. *Phys. Rev.* **1951**, *82* (2), 281–282. https://doi.org/10.1103/PhysRev.82.281.2.

(61) Lax, M. The Franck-Condon Principle and Its Application to Crystals. *J. Chem. Phys.* **1952**, *20* (11), 1752–1760. https://doi.org/10.1063/1.1700283.